Nucleating Effect of Expanded Graphite Nanoplatelets on Poly(Hydroxybutyrate)

Dana G. Miloaga, Hazel-Ann A. Hosein, Manjusri Misra, Lawrence T. Drzal
Composite Materials and Structures Center, Michigan State University
2100 Engineering Building, East Lansing, MI 48824

Introduction

Poly(hydroxyalkanoates) (PHAs)[1,2] are thermoplastic, biodegradable biopolyesters typically synthesized by various bacteria and microorganisms that use them as reserves of carbon and energy. [1-3] One of the most investigated PHAs is poly(hydroxybutyrate) (PHB) which, besides being biodegradable and biocompatible, is attractive due to its availability, processibility, and mechanical and barrier properties which are comparable to isotactic polypropylene and other synthetic polymers.[4,5] PHB is a highly crystalline thermoplastic that can be extruded, injection molded, and spun[6,7] without modifying traditional polymer processing equipment. It also has a low elongation at break (less than 10 %), an impact strength of 3 J/mm^2, a modulus of 1.7 GPa and a fracture stress of 35 MPa.[8] Despite having these characteristics, PHB is not widely applied in the manufacturing industry because of its inherent brittleness and narrow processibility window. The brittleness of PHB[8,9-12] is known to stem from three factors: a glass transition temperature close to room temperature, secondary crystallization occurring upon storage at room temperature, and an extremely low nucleation density, which all derive from the high purity of PHB and its stereochemical regularity.[10] There is an ongoing research thrust to discover efficient nucleating agents for PHB and its copolymers. Efficient nucleating agents would increase the polymer's crystallization temperature, and the crystallization rates, and generate smaller and more numerous spherulites, leading to materials with increased mechanical properties. In addition micro- and nanosized inorganic particles, like clay[14,15] and carbon nanotubes[16,17], may have the added advantage of acting as reinforcements for the polymer.

We report here on the nucleating effect of expanded graphite nanoplatelets (xGnP) on PHB. Graphite has a similar structure to boron nitride, and can be intercalated and exfoliated into very thin nanosized platelets[18] with extremely high surface area and in-plane stiffness as high as 1060 GPa.[19] The nonisothermal crystallization of PHB from the melt was examined, since a fundamental understanding is essential for optimizing the processing conditions for thermoplastic materials under dynamic conditions like extrusion and injection molding.[13,20-22] A kinetic analysis of the nonisothermal crystallization from melt was undertaken using models based on modifications of the Avrami equation. Optical microscopy and atomic force microscopy were used to characterize the morphology of PHB/xGnP systems and to offer further insight on the crystallization process.[23-25]

Experimental Section

Materials

Poly(hydroxybutyrate) was obtained from Metabolix (Cambridge, MA), and used without further purification. The expanded graphite nanoplatelets having an average size of

1 μm (xGnP-1) were obtained in-house[18,26] starting from GraphGuard™ 160-50A expandable graphite purchased from Graftech (Cleveland, OH).

Sample preparation

Samples of pure PHB and PHB containing, 0.01 % wt, 1 % wt, and 3 % wt xGnP-1 were prepared by extrusion followed by injection molding. The dried PHB powder was mixed with the xGnP-1 and extruded using a DSM micro-extruder (15 cm^3 capacity) (DSM Research B.V., The Nederlands). The temperatures in the three heating zones of the micro-extruder were 175 ^oC, 185 ^oC, and 195 ^oC respectively. The mixtures were extruded at 100 rpm, and the cycle time was three minutes. The extruded polymer systems were transferred through a cylinder preheated at 190 ^oC to a mini-injection molder in which the mold temperature was fixed at 50 ^oC. The injection molded flexural bars obtained were placed in sealed polyethylene bags in order to reduce moisture absorption.

Methods

Thermal analysis: differential scanning calorimetry (DSC). The melting and crystallization behavior of PHB/xGnP-1 samples were investigated using a 2920 Modulated DSC (TA Instruments). The runs were performed under nitrogen flow, after calibrating the DSC instrument using an Indium standard. For each run, a fresh sample (5-8 mg) of polymer was heated from room temperature to 190 ^oC, kept isothermal for five minutes, in order to remove the thermal history, then cooled to –60 ^oC, reheated to 190 ^oC, and cooled to room temperature. Six different heating/cooling rates were used: 5, 8, 10, 14, 17, and 20 ^oC/minute, and the data recorded during the second cooling step were analyzed.

Optical microscopy (OM). The samples for optical microscopy were prepared as thin polymer films by heating very thin sections of PHB/xGnP-1 injection molded bars in a Mettler Toledo FP82 hot stage, at a rate of 20 ^oC/minute from room temperature to 190 ^oC, kept isothermal for three minutes, then either allowed to crystallize upon cooling to room temperature, or to crystallize isothermally at different preset crystallization temperatures. The morphology of PHB and the size of the spherulites were observed using an Olympus BH2 optical microscope equipped with a Spot™ camera.

Atomic force microscopy (AFM). Thin polymer films were prepared as described for optical microscopy, using the Mettler Toledo FP80 hot stage. All images were collected on a Nanoscope™ IV instrument (Veeco, CA) equipped with a *J* scanner in tapping mode.

Results and Discussion

Crystallization of PHB in the presence of xGnP-1. The nonisothermal crystallization from the melt of pure PHB and PHB containing 1 % wt, and 3 % wt xGnP-1 was studied using differential scanning calorimetry. The melting temperature (T_m), the onset and end of crystallization temperatures (T_0 and T_∞), the temperature of the crystallization peak (T_p), the enthalpies of fusion and the crystallization enthalpies (ΔH_f and ΔH_c) were recorded for heating/cooling at six different rates ($D = 5, 8, 10, 14, 17$) and 20 ^oC/minute respectively).

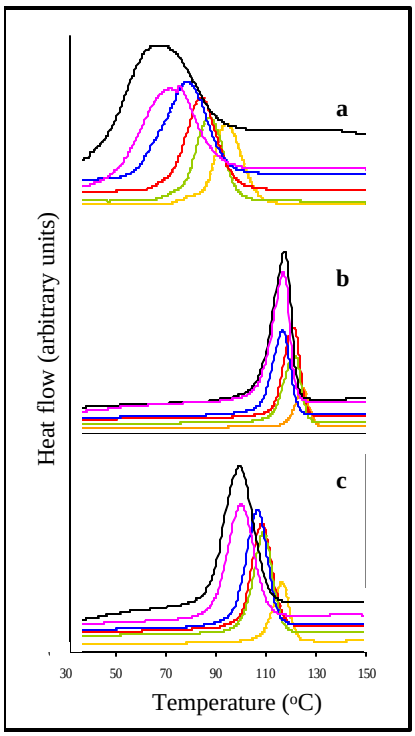

Figure 1. Nonisothermal crystallization curves obtained for (a) pure PHB, (b) PHB/ 1% xGnP-1 and (c) PHB/3 % xGnP-1 at six cooling rates: 5, 8, 10, 14, 17 and 20 °C/minute respectively.

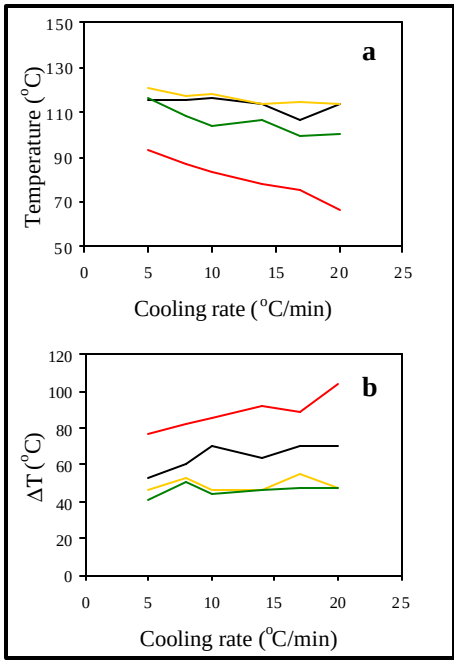

Figure 2. Graphs showing (a) the crystallization temperatures and (b) the degrees of supercooling versus cooling rate for pure PHB (–), PHB/0.01 % xGnP-1 (–), PHB/ 1% xGnP-1 (–), and PHB/3 % xGnP-1 (–).

Figure 1 shows the nonisothermal crystallization curves for the PHB/xGnP-1 systems described above. After the addition of xGnP-1, the crystallization peaks shifted to higher temperatures, which was the first indication of the nucleating effect ox xGnP-1. The crystallization peaks also became narrower, which suggested that PHB spherulites formed in the presence of xGnP-1 were smaller than the spherulites formed by the neat polymer.[17]

The graphs in Figure 2a show the values of T_p recorded for PHB containing different concentrations of xGnP-1, at different cooling rates. Figure 2b indicates that for PHB/xGnP-1 systems, the degrees of supercooling (defined as the difference between the melting temperature and the temperature of the crystallization peak, $\Delta T = T_m - T_p$) were lower than that of pure PHB. Both the shifts of the crystallization peaks and the decreases of the degree of supercooling are evidence of the nucleating effect of xGnP-1. The nucleating effect of graphite nanoplatelets was more evident at lower concentrations. A kinetic analysis of the nonisothermal crystallization from melt was performed using a modified form of the Avrami equation.[16,20-22,27-30]

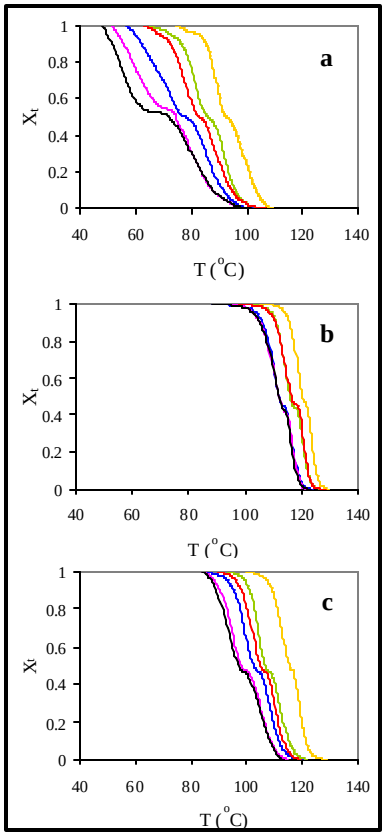

Figure 3. Development of relative crystallinity with temperature at different cooling rates for (a) pure PHB (b) PHB/1 % xGnP-1 (c) PHB/3 % xGnP-1.

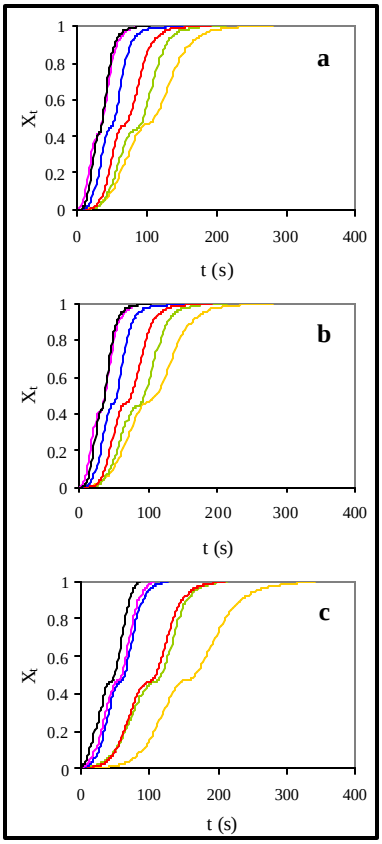

Figure 4. Development of relative crystallinity with time at different cooling rates for (a) pure PHB (b) PHB/1 % xGnP-1 (c) PHB/3 % xGnP-1.

The development of relative crystallinity with temperature for the PHB/xGnP-1 systems investigated is presented in Figure 3. In each of the three cases, after adding xGnP-1 to PHB, complete crystallization was achieved over a narrower temperature range, and in a shorter time. (Figure 4) The *S*-shaped curves indicate that pure PHB crystallizes in two steps. This phenomenon, also observed for ethylene terephtalate-ethylene oxide segmented copolymers,[21] is explained in terms of an initial fast growth phase of the crystals in an amorphous environment, followed by a slower growth phase as the crystals begin to impinge on each other in the interlamellar region.

The kinetic parameters for the nonisothermal crystallization from the melt of PHB/xGnP-1 samples were determined by plotting $\log[-\ln(1-X_t)]$ versus $\log t$ (Figure 5). For pure PHB, and PHB containing 1 % wt and 3 % wt xGnP-1, the curves were linear at first and then deviated from linearity, due to secondary crystallization.[20] However, for systems containing 0.01 % wt xGnP-1, the plots were not linear, possibly due to non-uniform dispersion of xGnP-1 in PHB, and these samples were not further subjected to kinetic analysis. The values of the kinetic parameters n, Z, and Z_c for neat PHB, and for PHB containing 1 % wt and 3 % wt xGnP-1 were obtained from the slopes and intercepts of the lines in Figure 5.

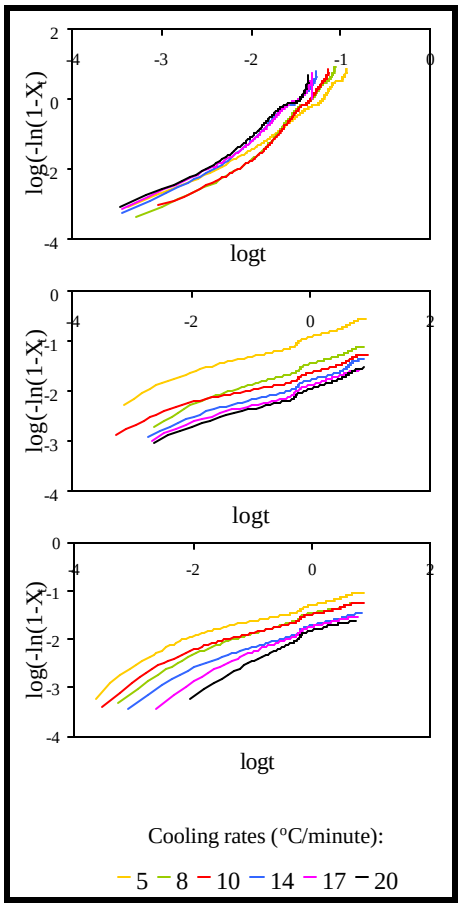

Figure 5. Graphs showing the results of modified Avrami analysis for (a) PHB (b) PHB/1 % xGnP-1 and (c) PHB/3 % xGnP-1 at six cooling rates: - 5 ^{o}C/minute; - 8 ^{o}C/minute; - 10 ^{o}C/minute; - 14 ^{o}C/minute; - 17 ^{o}C/minute and - 20 ^{o}C/minute.

According to the modified Avrami analysis, the rate of crystallization of pure PHB increased with increasing cooling rate (Figure 6). For PHB samples containing 1 % wt and 3 % wt xGnP-1, the crystallization rate parameters were higher than for pure PHB, but were independent of the cooling rate. Our results show that the time required to achieve half of the final crystallinity ($t_{1/2}$), as well as the maximum crystallization time, were higher for pure PHB than for PHB containing expanded graphite nanoplatelets (Figure 7, a, b).

The activation energies for the nonisothermal crystallization from melt were determined using the Kissinger method (equation (1))[20,30] based on the peak temperatures recorded by DSC:

$$\frac{d\left(\ln\left(\frac{D}{T_p^2}\right)\right)}{d\left(\frac{1}{T_p}\right)} = -\frac{\Delta E}{R}, \qquad (1)$$

where R is the universal gas constant, ΔE is the activation energy, and the other parameters are as defined previously. The activation energies were calculated using the slopes of the

lines obtained by plotting $\log\left(\frac{D}{T_p^2}\right)$ vs $\frac{1}{T_p}$. For PHB, PHB/1 % wt xGnP-1, and PHB/3 % wt xGnP-1, the activation energies were found to be –60.41 kJ/mol, –213.61 kJ/mol, and –101.86 kJ/mol respectively. ΔE for the nonisothermal crystallization from melt of PHB was in agreement with the value of -64.6 kJ/mol reported by An *et al*.[13]

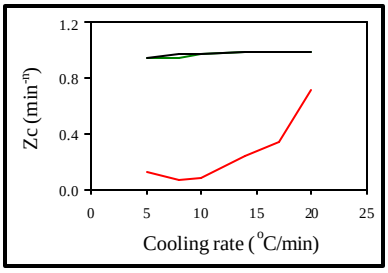

Figure 6. Nonisothermal crystallization rate parameters for pure PHB (–), PHB/1% xGnP-1 (–), and PHB/3 % xGnP-1 (–) systems, determined according to modified Avrami analysis.

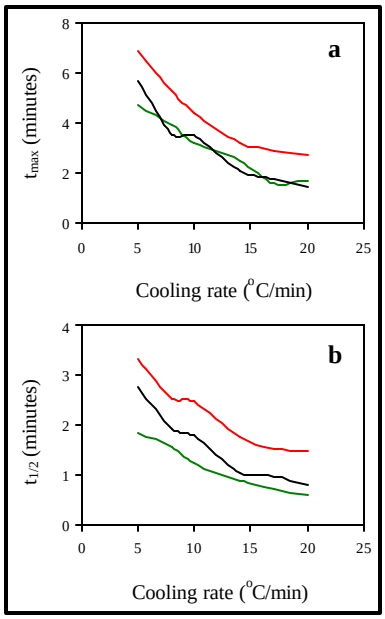

Figure 7. Graphs showing (a) the half-time crystallization times and (b) the maximum crystallization times for pure PHB (–), PHB/1% xGnP-1 (–), and PHB/3 % xGnP-1 (–) systems, determined according to modified Avrami analysis.

Morphology of PHB/xGnP-1 system

Optical microscopy was used to observe the distribution and growth of the crystallites formed by pure PHB and PHB/xGnP-1 systems during nonisothermal cooling from the melt, and their morphologies after crystallization. Figure 8 shows optical micrographs of the well-defined banded spherulitic structures (average radius of 70 µm) formed from pure PHB, and the much smaller spherulites formed in the presence of 0.01 % xGnP-1. For higher concentrations of PHB (1 % and 3 %), small spherulites crystallized spontaneously from the melt and formed agglomerates. This result was not unexpected since the higher concentrations of xGnP-1 introduced many heterogeneous nuclei which initiated nucleation of the PHB at 110-113 °C.

AFM images were collected for the pure PHB, and PHB containing 0.01 % wt, 1 % wt and 3 % wt xGnP-1 (Figure 9). Figure 9a shows an AFM height image of a PHB spherulite formed upon nonisothermal crystallization of PHB from the melt, having an approximate diameter of 90 µm, which is most likely an overestimation due to tip convolution effects. Figure 11b shows an AFM height image for a spherulite formed from the PHB/0.01 % wt xGnP-1 system also having a diameter of about 90 µm. In the case of the PHB/xGnP-1 systems

having higher concentrations of graphite nanoplatelets, the crystallites formed appeared to be much smaller and impinged upon each other (Figure 9b,c), so despite the accuracy of AFM, due to the nature of the sample, it was difficult to determine the exact sizes of the spherulites.

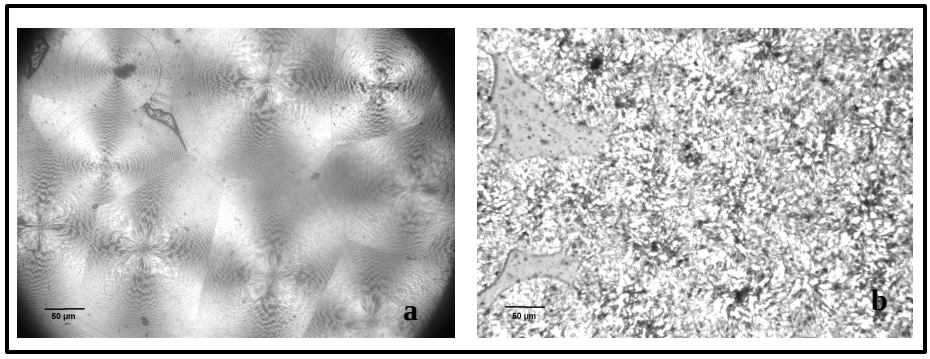

Figure 8. Optical micrographs showing spherulites of (a) pure PHB and (b) PHB/ 0.01 % wt xGnP-1 formed during nonisothermal crystallization from the melt.

Our AFM results indicate that the lamellar thickness of pure PHB spherulites crystallized from the melt ranges from 7 to 20 nm, as shown in the cross-sectional analysis in Figure 10a. The lamellar structure was also observable in the PHB/1 % wt xGnP-1 system at small scan sizes (250×250 nm) (Figure 10b), and the thickness was measured to be approximately 5 nm. On the other hand, AFM images of PHB/3 % wt xGnP-1 samples revealed an apparent disruption of the lamellar structure, attributable to the wide distribution of xGnP-1 throughout the crystalline structure (Figure 11).

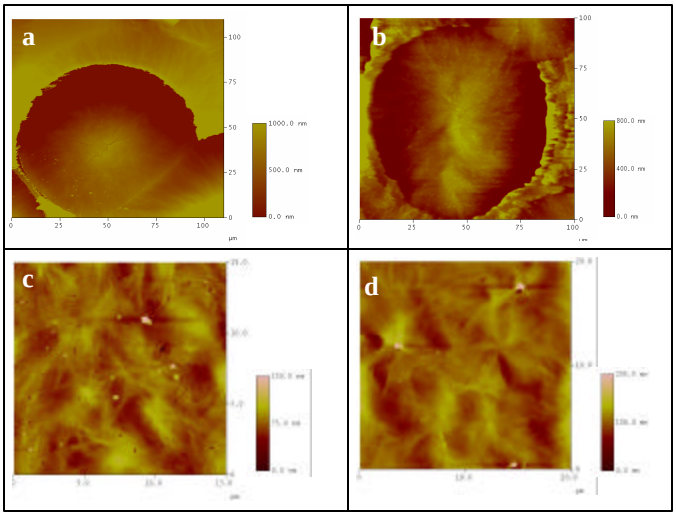

Figure 9. AFM tapping mode height images (top view) showing spherulites of (a) pure PHB and PHB containing (b) 0.01 % wt xGnP, (c) 1 % wt xGnP and d) 3 % wt xGnP.

Overall, our results indicate that the lamellar thickness decreased as the amount of xGnP-1 increased, and was proportional to the size of the crystalline structures formed. These experimental results are consistent with calculated values[27] for lamellar thicknesses, which ranged from 17 to 24 nm.

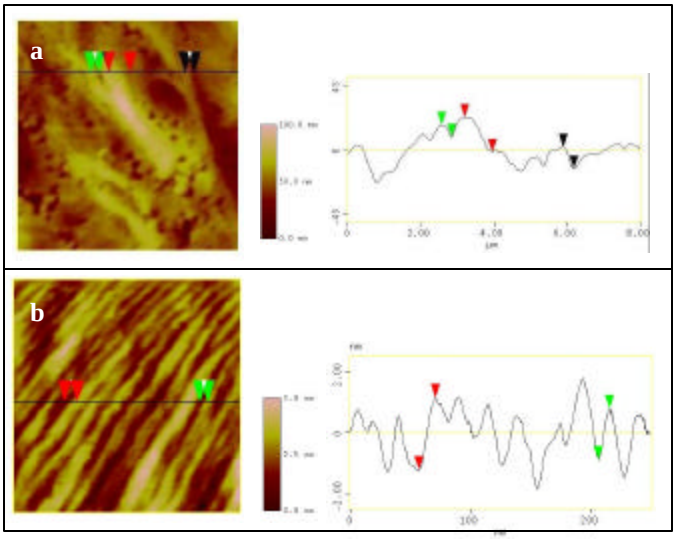

Figure 10. AFM tapping mode height images (top view) and accompanying cross-sections showing the lamellar thicknesses of spherulites of (a) pure PHB and (b) PHB/1 % wt xGnP-1.

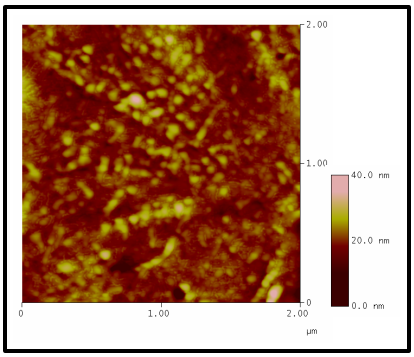

Figure 11. AFM height image (top view) of PHB/3 % xGnP-1 showing the apparent disruption of the lamellar structure of the polymer.

Conclusions

We have shown that expanded graphite nanoplatelets efficiently nucleate PHB, leading to systems that crystallize from the melt faster and at higher temperatures. This thermal behavior is particularly desirable for dynamic processing conditions such as extrusion and injection molding, which are largely utilized for obtaining biocomposites. Very small amounts of xGnP-1 (0.01 % wt) increased the crystallization temperature of PHB by approximately 30 ^{o}C, leading to the formation of smaller spherulites, as evidenced by optical microscopy and atomic force microscopy. A modified form of the Avrami equation accurately described the nonisothermal crystallization from the melt of PHB/xGnP-1 systems, and showed that this process occurred faster for PHB/xGnP-1 systems than for pure PHB. The pure polymer crystallized faster as the cooling rate increased, while the rates of crystallization for the PHB/xGnP-1 systems from the melt were almost independent of the cooling rate. Additionally, nonisothermal crystallization from the melt was shown to be more energetically favored for the systems containing xGnP than for pure PHB. Maximum crystallinity was also achieved faster in PHB/xGnP-1 systems than in pure PHB. Although, the kinetic analysis and

activation energies indicate that 3 wt % xGnP in PHB is excessive for initiating nucleation, it should be noted that the excess xGnP may act as reinforcement, thereby leading to enhanced mechanical properties and possibly inducing electrical conductivity in the bio-nanocomposites. The effects of xGnP on the crystallization behavior and morphology of PHB provide a foundation for further investigations of PHB/xGnP systems, in the view of obtaining advanced bio-nanocomposites with controllable thermal and mechanical properties, and electrical conductivity. Investigations of the mechanical properties of these PHB/xGnP-1 nanocomposites are the focus of ongoing research and our preliminary results indicate improvements in impact and flexural properties compared to the neat polymer.

Acknowledgements

Funding from the US Environmental Protection Agency (EPA) Science to Achieve Results (STAR) program (award RD 8309040) is greatly appreciated. The authors would also like to thank Metabolix Inc. (Cambridge, MA) for providing the poly(hydroxybutyrate) used in this research.

References

1. Dorgan, J.R.; Lehermeier, H.J.; Palade, L.-I.; Cicero, J. *Macromol. Symp.* **2001**, *175*, 55-66.
2. Tokiwa, Y.; Calabia, B. *Biotechnol. Lett.* **2004**, *26*, 1181-1189.
3. Lenz, R.W.; Marchessault, R.H. *Biomacromolecules* **2005**, *6*, 1-8.
4. Chen, G. G-Q. In *Biodegradable Polymers for Industrial Applications*, 1st Ed.; Smith, R., Ed.; Woodhead Publishing Limited: Cambridge, England, 2005, p. 32-51.
5. Satkowski, M.M.; Melik, D.H.; Autran, J.-P.; Green, P.R; Noda, I.; Schechtman, L.A. In *Biopolymers*, Steinbüchel, A., Doi, Y., Eds., Wiley-VCH: Wienheim, 2001, 231.
6. Gordeyev, S.A.; Nekrasov, Y.P. *J. Mater. Sci Lett.* **1999**, *18*, 1691-1692.
7. Gordeyev, S.A.; Nekrasov, Y.P.; Shilton, J. *J. Appl. Polym. Sci.* **2001**, *81*, 2260-2264.
8. Briassoulis, D. *J. Polym. Env.* **2004,** *12(2)*, 65-81.
9. de Koning, G.J.; Lemstra, P.J. *Polymer* **1993**, *34(19)*, 4089-4094.
10. de Koning, G.J.M.; Scheeren, A.H.C.; Lemstra, P.J.; Peters, M.; Reynaers, H. *Polymer* **1994**, *35(21)*, 4598-4605.
11. Barham, P.J.; Keller, A.; Otun, E.L. *J. Mater. Sci.* **1984**, *19*, 2781-2794.
12. El-Hadi, A.; Schnabel, R.; Straube, E.; Muller, G.; Henning, S. *Polym. Test.* **2002**, *21*, 665-674.
13. An, Y.; Dong L.; Mo, Z.; Liu, T.; Feng, Z. *J. Polym. Sci. Polym. Phys.* **1998**, *36*, 1305-1312.
14. Krishnamoorti, R.; Vaia, R.A.; Giannelis, E.P. *Chem. Mater*. **1996**, *8*, 1728-1734.
15. Park, H-M.; Liang, X.; Mohanty, A.K.; Misra, M.; Drzal, L.T. *Macromolecules* **2004**, *37*, 9076-9082.
16. Grady, B.P.; Pompeo, F.; Shambaugh, R.L.; Resasco, D.E. *J. Phys. Chem. B*. **2002**, 106, 5852-5858.
17. Lai, M.; Li, J.; Yang, J.; Liu, J.; Tong, X.; Cheng, H. *Polym. Int.* **2004**, *53*, 1479-1484.
18. Fukushima, H. *Graphite Nanoreinforcements in Polymer Nanocomposites*, Ph.D. Thesis, Michigan State University, **2003**.
19. Ruoff, R.S.; Ding, W.; Piner, R.; Stankovich, S. *Polym. Mat.: Sci & Eng.* **2005**, *92*, 511.
20. Liu, T.; Mo, Z.; Zhang, H. *Polym. Eng Sci.* **1997**, 3*7(3)*, 568-575.
21. Kong, X.; Yang, X.; Zhou, E.; Ma, D. *Eur. Polym. J.* **2000**, *36*, 1085-1090.
22. Kim, J.Y.; Park, H.S.; Kim, S.H. *Polym. Mat.: Sci. Eng.* **2005**, *92*, 478-479.
23. Ichikawa, M.; Nakamura, K.; Yoshie, N.; Asakawa, N.; Inoue, Y. *Macromol. Chem. Phys.* **1996***, 197,* 2467-2480*.*
24. Hobbs, J.K.; Binger, D.R.; Keller, A.; Bahram, P.J. *J. Polym. Sci.: B* **2000**, *38*, 1575-1583.
25. Gazzano, M.; Focarete, M.L.; Riekel, C.; Scandola, M. *Biomacromolecules* **2000**, *1*, 604-608.
26. Cho, D.; Lee, S.; Yang, G.; Fukushima, H.; Drzal, L.T. *Macromol. Mater. Eng*. **2005**, *290*, 179-187.
27. Avrami, M. *J. Chem. Phys*. **1939**, *7*, 1103-1112.
28. Avrami, M. *J. Chem. Phys*. **1940**, *8*, 212-224.
29. Liu, T.; Mo, Z.; Zhang, H. *J. Appl. Polym. Sci* **1998**, *67*, 815-821.
30. Jeziorny, A. *Polymer* **1978**, *19(10)*, 1142-1144.